

A Study of a Retrieval Method for Temperature and Humidity Profiles from Microwave Radiometer Observations Based on Principal Component Analysis and Stepwise Regression

HAOBO TAN,* JIETAI MAO,⁺ HUANHUAN CHEN,[#] P. W. CHAN,[@] DUI WU,[#] FEI LI,* AND TAO DENG*

* *Institute of Tropical and Marine Meteorology, CMA, Guangzhou, China*

⁺ *Department of Atmospheric Science, Peking University, Beijing, China*

[#] *Institute of Tropical and Marine Meteorology, CMA, and School of Environmental Science and Engineering, Sun Yat-sen University, Guangzhou, China*

[@] *Hong Kong Observatory, Hong Kong, China*

(Manuscript received 13 April 2010, in final form 1 October 2010)

ABSTRACT

This paper discusses the application of principal component analysis and stepwise regression in the retrieval of vertical profiles of temperature and humidity based on the measurements of a 35-channel microwave radiometer. It uses the radiosonde data of 6 yr from Hong Kong, China, and the monochromatic radiative transfer model (MonoRTM) to calculate the brightness temperatures of the 35 channels of the radiometer. The retrieval of the atmospheric profile is then established based on principal component analysis and stepwise regression. The accuracy of the retrieval method is also analyzed. Using an independent sample, the root-mean-square error of the retrieved temperature is less than 1.5 K, on average, with better retrieval results in summer than in winter. Likewise, the root-mean-square error of the retrieved water vapor density reaches a maximum value of 1.4 g m^{-3} between 0.5 and 2 km, and is less than 1 g m^{-3} for all other heights. The retrieval method is then applied to the actual measured brightness temperatures by the 35-channel microwave radiometer at a station in Nansha, China. It is shown that the statistical model as developed in this paper has better retrieval results than the profiles obtained from the neural network as supplied with the radiometer. From numerical analysis, the error with the water vapor density retrieval is found to arise from the treatment of cloud liquid water. Finally, the retrieved profiles from the radiometer are studied for two typical weather phenomena during the observation period, and the retrieved profiles using the method discussed in the present paper is found to capture the evolution of the atmospheric condition very well.

1. Introduction

The measurement of the atmospheric temperature and water vapor profiles is very important in a number of areas, such as meteorology, communication, and aviation. It has long been made using upper-air ascents. However, these ascents are only available twice a day and the upper-air stations are separated by about 300 km. In certain meteorological applications, the existing upper-air measurements may not provide sufficient information (Westwater et al. 2005a). Nowcasting is a typical example. Other examples include the monitoring of such

mesoscale phenomena as the passage of frontal systems and the development of convective clouds. These weather events occur within a short period of time and the evolution of atmospheric profiles may not be captured successfully by the conventional upper-air ascents. Accurate information with high temporal resolution would be necessary for studying these phenomena. Ground-based microwave radiometers may provide the required information with high precision and sufficient temporal resolution. They also have the advantage of being portable as well as running continuously, unattended, from several months up to a year. As a result, radiometers have become useful remote sensing tools for atmospheric profiling (Hogg et al. 1983a; Marzano et al. 2002). They have found extensive applications in a variety of areas, including meteorological observations, forecasting, communication, satellite correction, climatology,

Corresponding author address: Haobo Tan, Institute of Tropical and Marine Meteorology, China Meteorological Administration, Guangzhou 510080, China.
E-mail: hbtan@grmc.gov.cn

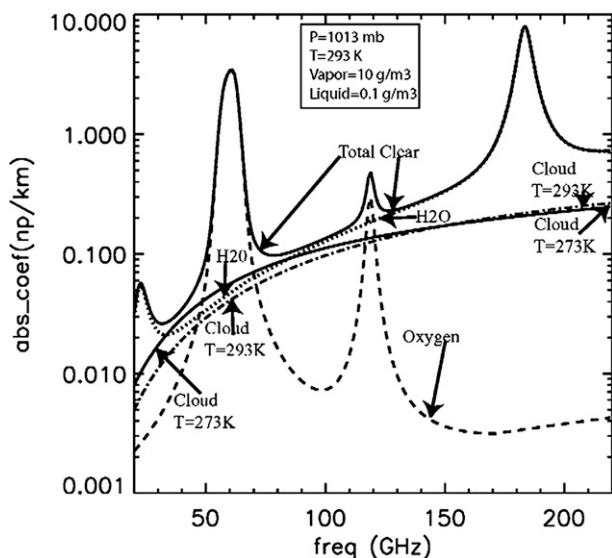


FIG. 1. Atmospheric absorption bands of microwave radiation between 20 and 220 GHz.

air-sea interaction, fundamental molecular physics, and real-time correction of the refraction of electromagnetic waves (Hogg et al. 1983b; Liljegren 2000; Ware et al. 2003; Westwater et al. 2004).

In microwave remote sensing of the atmosphere, the characteristics of microwave radiation depend on the absorption of the waves by the atmosphere. According to modern light theory and experimental results, the major absorbing matter of microwave radiation in the atmosphere include water vapor, oxygen, cloud liquid water, and precipitation. As shown in Fig. 1, there are two absorption bands of microwave radiation by water vapor in the frequency range of 10–220 GHz, namely, near 22 and 183 GHz. The absorption bands of oxygen occur in the region near 60 and 119 GHz. The absorption of the microwave radiation by cloud liquid water is continuous across the 10–220-GHz spectrum. According to Kirchhoff's law, a radiator that has the strongest absorption in a frequency band also has the strongest emission in that band. As a result, the changes of the microwave radiation in the frequency region around 22.235 GHz mainly reflect the evolution of atmospheric water vapor density. Similarly, the radiation changes in the strong absorption bands of oxygen near 60 GHz show the evolution of atmospheric temperature, and those occurring in the frequency band near 31.5 GHz are mainly related to the evolution of the liquid water paths inside clouds (Hogg et al. 1983b). Based on the above principles, the microwave radiometer working in the above-described frequency bands could be used to measure the vertical profiles of temperature, water vapor, and liquid water in the atmosphere. The retrieval method of such profiles is also under continuous development.



FIG. 2. The ground-based, 35-channel microwave radiometer.

There are two major types of retrieval method, namely, physical calculation and statistical analysis. Physical calculation involves extensive computation and is thus time consuming. On the other hand, the statistical method is relatively simple. Westwater et al. (2005b) described the latter retrieval method in detail and pointed out that the accuracy of the retrievals could be improved by incorporating results of numerical weather prediction models or using a large amount of historical data through statistical analysis. Recently, some new statistical methods have been introduced with reasonably good results, including the neural network (Churnside et al. 1994), Kalman filter (Ledskam and Staelin 1978), genetic algorithm (Lin et al. 1997), and Bayesian maximum probability estimation (Solheim et al. 1998). However, generally speaking, the regression method (Phillips et al. 1979; Zhao et al. 1984; Lü et al. 1993; Wei and Lu 1994; Duan and Wu 1999) is still considered to be the most common and effective retrieval algorithm for microwave radiometers. Moreover, with the advancement of radiometer hardware and the increase of the number of observation channels, the regression method is expected to better capture the complicated nonlinear relationship between the measured brightness temperatures and the retrieved atmospheric quantities, and thus the retrieval results could be further improved.

In 2007, the Institute of Tropical and Marine Meteorology of the China Meteorological Administration introduced a 35-channel microwave radiometer from Radiometrics (Fig. 2). It includes 21 frequency channels of K band between 22 and 30 GHz and 14 channels of V band between 51 and 59 GHz. Apart from these 35 channels, it also has sensors for surface temperature, relative humidity, and pressure as manufactured by Vaisala,

an infrared radiometer to measure the cloud-base temperature, a rain detector, and a blower for removing dust and rainwater from the radome of the radiometer. This instrument generates data files of 3 levels, namely, level-0 (LV0) data of voltages, level-1 (LV1) data of brightness temperatures of the frequency channels, and level-2 (LV2) data of retrieved profiles of temperature, humidity, water vapor density, and liquid water based on the Stuttgart neural network [the recurrent neural network (RNN) method]. This paper simulates the brightness temperatures at the 35 frequency channels using upper-air ascent data of 6 yr in combination with the monochromatic radiative transfer model (MonoRTM), and establishes their relationship with the vertical profiles of temperature and humidity based on principal component analysis (PCA) and the stepwise regression method. The accuracy of this retrieval method would be determined by making reference to the actual upper-air ascent measurements, compared with those achieved by the RNN method.

This paper consists of the following six parts: introduction, data, methodology, retrieval results, case studies, and discussion and conclusions. The third part presents stepwise regression equations and retrieval evaluation using an independent data sample. The fourth part then uses measured brightness temperatures from the 35-channel microwave radiometer for retrieval of atmospheric profiles, and discusses the comparison with upper-air ascent data and retrieval results of the RNN method. Emphasis would be put on the accuracy of the retrieval of temperature, relative humidity, and water vapor density. The fifth part discusses the retrieval results in two typical weather phenomena over southern China.

2. Data

The data used in the present study include the radiosonde data from Hong Kong, China, at 0000 and 1200 UTC every day between June 2003 and August 2009, as well as the LV1 and LV2 data from the 35-channel microwave radiometer at Nansha, China, between September and November 2008. The radiometer site (5-m altitude) at Nansha is located at about 77 km northeast of the radiosonde launch site at King's Park (59-m altitude).

3. Methodology

a. Radiative transfer model

According to the radiative transfer equation of atmospheric microwave radiations, the brightness temperature of the radiation received at the ground for the zenith angle θ is given by

$$TB(\theta, \lambda) = T_{\infty} e^{-\int_{\infty}^{p_0} \alpha \sec\theta dp} + \int_{p_0}^{\infty} T(p) \alpha e^{-\int_p^{p_0} \alpha \sec\theta dp} \sec\theta dp. \quad (1)$$

In Eq. (1), the first term on the right-hand side refers to the cosmic radiation in the background after attenuation in the atmosphere; the second term is the radiation emitted from the atmosphere to the ground. The quantity T_{∞} is the cosmic background temperature and it is usually taken to be 2.75 K. Here, T_p is the atmospheric temperature at the pressure level p ; p_0 is the surface pressure; and α is the atmospheric absorption coefficient at frequency λ , mainly resulting from absorptions by oxygen molecules, water vapor, and liquid water.

We use MonoRTM (Clough et al. 2005; Boukabara et al. 1999) to solve Eq. (1). This model employs the same physical mechanisms as the line-by-line radiative transfer model (LBLRTM). However, it allows the calculation of selected frequencies only and thus makes the computation faster while maintaining reasonable accuracy. Moreover, the model takes into account the impact of microwave absorption by cloud liquid water. Cimini et al. (2004) contains the verification and comparison of results obtained by four radiative transfer models using ground-based, remote sensing observations of brightness temperatures, and it is found that MonoRTM simulates the brightness temperatures of microwave radiations very well.

b. Principal component analysis and stepwise regression

When the regression method is used in forecasting, there could be a number of predictors that may not be mutually independent but rather are related to each other to a certain extent. In such situations, the PCA could be used to transform these predictors into a group of mutually independent factors. As a result, the signals are made to exist in a reduced set of forecasting factors, and PCA is a methodology of dataset simplification. At the same time, PCA is also a linear transformation that puts the dataset in a new coordinate system in which the projected data with the largest variance occurs at the first axis (i.e., the first principle component); the projected data with the second largest variance appears at the second axis (i.e., the second principle component), etc. PCA effectively reduces the dimensions of the input dataset, while it keeps those input data with the largest contributions to the variance. Regression is a statistical method used to find out the relationship between the predictors and predictands. Stepwise regression allows the introduction of predictors progressively according to their statistical significance. The originally introduced predictors may be removed from the regression equation

following the introduction of new predictors because the former may no longer be statistically significant anymore. Through this process, only the important predictors are included in the equation obtained at the end of the stepwise regression (Shi 2002).

The MP-3000A microwave radiometer in use has as many as 35 frequency channels that are not mutually independent. To establish a reasonable and stable regression equation, we consider a total of 38 predictors in the PCA and stepwise regression, namely, brightness temperatures from the 35 frequency channels as well as 3 surface meteorological parameters (temperature, relative humidity, and pressure). Cloud-base temperature data from a zenith infrared sensor are used to constrain neural network humidity retrievals. However, these data are not included in the PCA.

c. Establishment of retrieval algorithm and testing by an independent data sample

Calculated brightness temperatures for the 35 channels of the microwave radiometer are obtained by applying MonoRTM to radiosonde data of Hong Kong in the period from June 2003 to August 2009. The dataset has covered temperature and relative humidity profiles in a wide variety of weather conditions. However, the profiles of cloud liquid water as required in the calculation of brightness temperatures are not available in the conventional upper-air ascent data, and as such they are assumed to take the form noted in Wang et al. (1995). Namely, (i) cloud is taken to exist if relative humidity above 600 m is greater than or equal to 95%; (ii) fog is taken to exist if relative humidity below 600 m is greater than or equal to 95%; and (iii) the cloud liquid water is taken to be 0.26 g m^{-3} and the fog liquid water is taken to be 0.20 g m^{-3} in accordance with observational data over southern China in Wu (1987a,b) and Wu et al. (1998). The calculated brightness temperatures, taken as X1–X35, and the surface meteorological parameters, taken as X36–X38, are used as predictors. After normalization and PCA, these 38 predictors are transformed into 6 new predictors, named Z1–Z6, which are linear combinations of the original predictors. The new predictors are then correlated with the temperatures Tz_i and water vapor densities WVz_i of the various heights using the stepwise regression method. The vertical resolution is 50 m for the height between 0 and 0.5 km, 100 m between 0.5 and 2 km, and 250 m between 2 and 10 km. There are a total of 75 layers, and the matrix of regression coefficients is called B with the dimensions of $75 \times m$ ($m \leq 6$);

$$Tz_i = \sum_{j=1}^m (B_Tz_{ij} \times Z_j) \quad (i = 1, 2, \dots, 75; m \leq 6), \quad (2)$$

$$WVz_i = \sum_{j=1}^m (B_WVz_{ij} \times Z_j) \quad (i = 1, 2, \dots, 75; m \leq 6). \quad (3)$$

When brightness temperatures are input into the regression Eqs. (2) and (3), the vertical profiles of temperature and water vapor density are then obtained. To reflect the seasonal variation of the atmospheric conditions, the upper-air ascent data are classified into spring (March–May), summer (June–August), autumn (September–November), and winter (December–February) in the establishment of the respective regression equations. The accuracy of the retrieved profiles in different seasons is then studied separately. The sample sizes of the 4 seasons are 901, 1063, 915, and 898 (from spring to winter, respectively). The upper-air ascent data in the period from September 2008 to August 2009 are used as an independent dataset in the analysis of the performance of the regression equations, and thus they are not involved in the establishment of the equations. The accuracy of the retrieved profiles is determined by comparison with the actual radiosonde measurements in terms of the mean bias (MB) and root-mean-square error (RMSE). Let n be the size of the sample for comparison in each season. The actually measured value is taken as O_i (where i is the label of the sample). The retrieved value based on the regression equation is taken as R_i . The MB, RMSE, and normalized mean error (NME) of the retrieved value relative to the actual measured value are given by

$$MB = \frac{1}{n} \sum_{i=1}^n (R_i - O_i), \quad RMSE = \left[\frac{1}{n} \sum_{i=1}^n (R_i - O_i)^2 \right]^{1/2},$$

$$NME = \left(\sum_{i=1}^n |R_i - O_i| \right) / \sum_{i=1}^n O_i.$$

Figures 3 and 4 give the comparison results with the actual radiosonde measurements in the four seasons for the retrieved temperature and water vapor density values, respectively. At each height, the MB, RMSE, and NME between the two datasets are shown.

For temperature profiles, it could be seen from Fig. 3 that the retrieval results in the summer are better. For heights below 2 km, MB is about $\pm 0.1 \text{ K}$ and RMSE is less than 0.9 K. For heights between 2 and 10 km, MB is about $\pm 0.2 \text{ K}$ and RMSE is less than 1.2 K. The retrieval results are not as good in the winter. MB reaches 0.8 K for heights around 2.5 km and is about $\pm 0.6 \text{ K}$ for other heights. RMSE is less than 3.0 K for heights between 2 and 8 km, and less than 2.0 K for other heights. The accuracy of the retrieval results in autumn and spring lie between those of summer and winter. Overall,

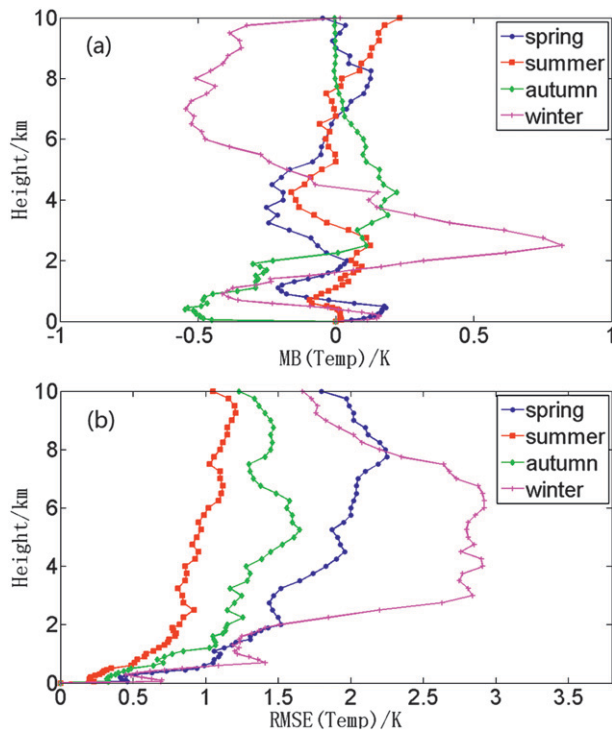


FIG. 3. Comparison results for the retrieved temperature profiles in the four seasons: (a) MB and (b) RMSE.

the performance of PCA plus stepwise regression is satisfactory in the retrieval of atmospheric temperature profiles. The retrieval accuracy is slightly better than some of the previous works reported in the literature (Askne and Westwater 1996). Temperature variation is higher in winter in Hong Kong, which may lead to slightly lower accuracy in the temperature retrieval in this season.

It could be seen from Fig. 4 that, in the retrieval of water vapor density, MB is larger below 2 km in all seasons. The bias is the largest in wintertime. The RMSE profiles in all seasons show a single peak in the troposphere. The RMSE is the largest at the heights between 0.5 and 2 km, reaching 1.4 g m^{-3} . It is less than 1 g m^{-3} for other heights. Compared with previous work in the literature (Askne and Westwater 1996; Guldner and Spankuch 2001; Liljegren et al. 2004; Hewison 2007; Liu et al. 2007), the error in the retrieval of water vapor density is larger in the current study. However, this comparison of the RMSE value may not be too meaningful because Hong Kong is situated at the south China coast with a relatively large amount of water vapor density in all seasons. In this regard, NME is used to study the magnitude of the error in the modeled results relative to the absolute value of the quantity under consideration, and it may be more meaningful for the study of the error

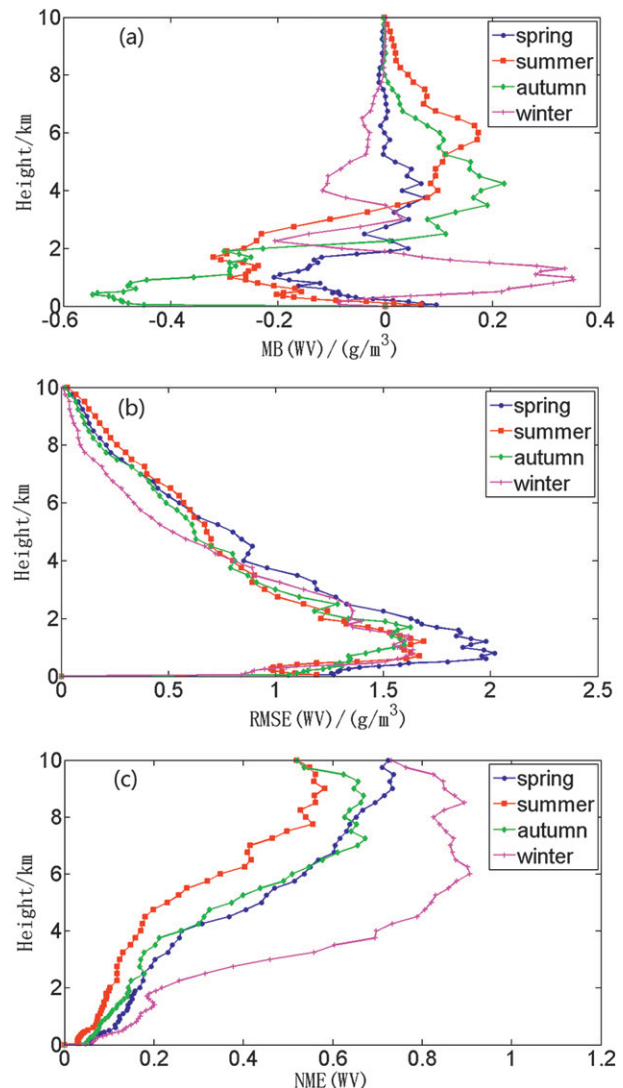


FIG. 4. Comparison results for the retrieved water vapor density profiles in the four seasons: (a) MB, (b) RMSE, and (c) NME.

in water vapor density retrieval. From Fig. 4c, NME is generally less than 0.2 for the layers with the higher water vapor density at the lower troposphere. As such, the accuracy of the retrieved water vapor density is considered to be basically acceptable. The RMSE is higher in the springtime, which may be due to the uncertainty associated with the cloud liquid water profile and the rapid fluctuations in the water vapor density around the onset of the summer monsoon.

4. Retrieval results

a. Comparison of different retrieval methods

The primary purpose of developing the PCA plus stepwise regression method (hereafter PSR method) is

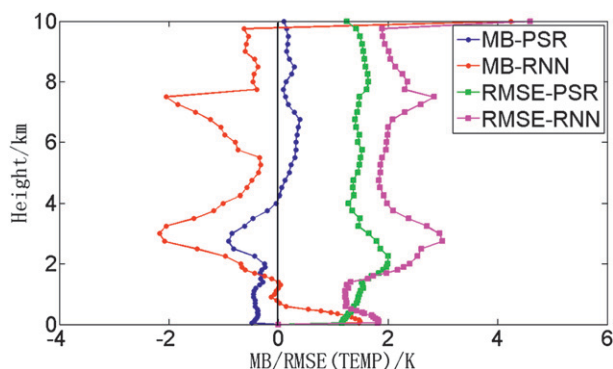


FIG. 5. Comparison results for temperature profiles.

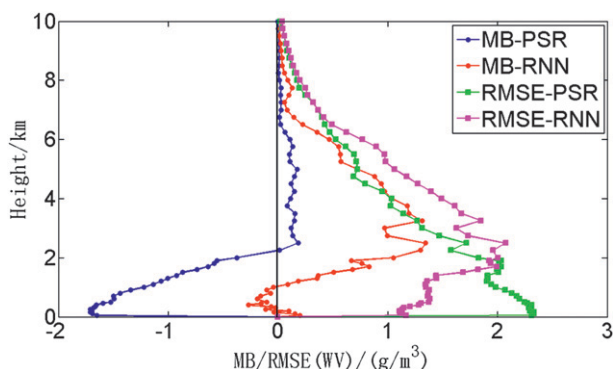


FIG. 6. Comparison results for water vapor density profiles.

to improve the retrieval results for the microwave radiometer in the actual applications. As such, we consider the actual measured data by the 35-channel radiometer at Nansha between September and November 2008. The PSR method is applied to such brightness temperature data to obtain the vertical profiles of temperature and water vapor density. The profiles are also obtained using the RNN method as supplied with the radiometer. The quality of the 2 sets of vertical profiles at the same time and height is studied in comparison with upper-air ascent data. It is expressed in terms of MB and RMSE for the retrieved temperature, water vapor density, and relative humidity.

Figures 5–7 give the comparison results of the two retrieval methods for temperature, water vapor density, and relative humidity, respectively, by using the upper-air ascent data as the truth.

It could be seen from Figs. 5–7 that, because of the separation (77 km) and height difference (5 versus 59 m) between the radiometer site and the radiosonde launch site, and the uncertainty inherent in the instruments, the errors of the retrieved temperature and water vapor profiles based on the actual measured brightness temperatures of the radiometer are larger than those obtained with the independent data sample (cf. Figs. 3 and 4). For temperature retrieval, both MB and RMSE for the PSR method are smaller than those of the RNN method, and thus the retrieved profiles are closer to the actual measurements (Fig. 5). On the other hand, the error of the PSR method in retrieving water vapor density is slightly larger than that of the RNN method. The RMSE is generally less than 2.0 g m^{-3} (Fig. 6). Using the retrieved temperature and water vapor density profiles, the relative humidity profile could also be obtained. For the two retrieval methods, MB and RMSE values are comparable for heights below 2.25 km. For heights aloft, the PSR method has smaller errors than the RNN method.

b. Identification of error source

From the above analysis, the quality of the retrieved water vapor density by the PSR method has yet to be improved. The accuracy of retrieval depends on a number of factors. This paper mainly focuses on the effect of cloud liquid water profiles on the retrieval of water vapor density profiles. From Fig. 1, it could be seen that the difference of the absorption coefficients between cloud liquid water and water vapor density in the K band is less than one order of magnitude. On the other hand, in the V band, the difference of the absorption coefficients between cloud liquid water and oxygen is larger. As a result, the vertical profile of cloud liquid water has a significant impact on the retrieval of water vapor density, whereas its effect on the retrieval of the temperature profile is smaller. Unfortunately, the vertical profile of cloud liquid water is not available in the conventional upper-air ascent data. We could only study the impact of the cloud liquid water profile on the retrieval of the water vapor density profile by assuming a number of prescribed forms of the former profile. The prescribed forms are described in Table 1.

Figure 8 shows the impact of the different prescribed forms of the cloud liquid water profile on the retrieval of

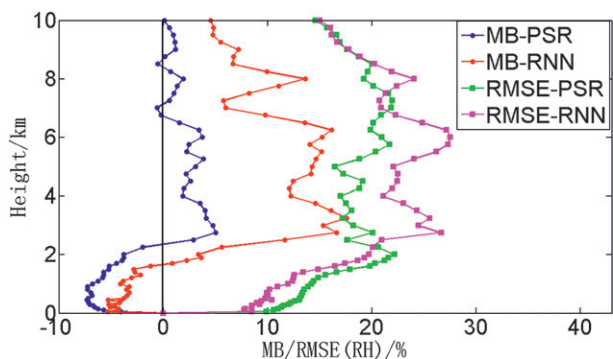


FIG. 7. Comparison results for relative humidity profiles.

TABLE 1. Prescribed forms of the vertical profile of cloud liquid water.

No.	Conditions	Liquid water density
0		No
1	85% < RH < 95%	0.01–0.2 g m ⁻³
	RH > 95%	0.5 g m ⁻³
2	RH > 85%	0.5 g m ⁻³
3	RH > 95%	0.01 g m ⁻³
4	RH > 95% and H > 0.6 km	0.20 g m ⁻³
	RH > 95% and H < 0.6 km	0.26 g m ⁻³

the water vapor density profile, expressed in terms of the variation of the correlation coefficient between the retrieved water vapor density and the actual measurement with height, and the RMSE. The amount of the cloud liquid water in the different prescribed forms follows the relationship No. 2 > No. 1 > No. 4 > No. 3 > No. 0. Among them, form No. 1 is based on Cady-Pereira et al. (2004). Form No. 4 is based on the work of Wu et al. (1987a,b) and Wu et al. (1998), which may be regarded as a more reasonable assumption about the cloud liquid water profile. Forms No. 2 and 3 take on rather extreme values. Form No. 0 does not consider the existence of cloud liquid water at all. From the study of the correlation coefficient and RMSE as given above, the retrieval results of water vapor density are the worse without taking into account the cloud liquid water. The retrieval results improve slightly for extreme values (i.e., either very large values or very small values) of cloud liquid water. The results are the best with the incorporation of the reasonable amount of cloud liquid water. As such, it could be seen that the existence of cloud liquid water and its vertical variation have a significant impact on the retrieval of the water vapor density profile. This impact does not simply scale monotonically with the amount of cloud liquid water under consideration. Moreover, if the upper-air ascent data contain the real profile of cloud liquid water, the retrieval of the water vapor density for the radiometer could be improved greatly.

5. Case studies

By applying the PSR method as discussed above, the radiometer observations in two typical weather phenomena over southern China are analyzed; namely, Typhoon Hagupit, during the period 23–24 September 2008, and the arrival of the cold monsoon surge, during the period 7–9 November 2008.

At 2245 UTC 23 September 2008, Typhoon Hagupit made landfall at Chencun, Dianbai County, Maoming City of Guangdong Province, China, bringing strong winds and heavy rain to the Pearl River delta region (Fig. 9). From Figs. 10a to 10c, between 1300 and 2100 UTC 23 September before the landfall of the typhoon, the southerly winds associated with the typhoon brought humid air to southern China. With the accumulation of water vapor, the relative humidity reached 80% or above in the troposphere. Between 2100 UTC 23 September and 0000 UTC 24 September during the landfall of the typhoon, no rain occurred at Nansha and water vapor density reached 15 g m⁻³ at the height of about 3 km. Relative humidity at the surface was above 90% at that time, and the troposphere was nearly saturated at heights between 2 and 8 km. In the period 0000–0700 UTC 24 September, there was rain at Nansha with the hourly rainfall reaching 270 mm at 0200 UTC (Figs. 10f,g). With the release of latent heat as water vapor condensed, there was a brief period of temperature increase at heights of 1–2 km. From 0800 UTC 24 September onward, both the temperature and the water vapor density over the troposphere started to decrease. The radiometer successfully captures the evolution of the thermodynamic profiles of the troposphere in the whole process.

The data from the rain detector of the radiometer are shown in Fig. 10f; “1” indicates the occurrence of rain, and “0” means no rain. There are vertical, narrow “bands” in the time–height plots of water vapor density and relative humidity during the occurrence of rain. Such rapid fluctuations in the water vapor density and relative humidity profiles may be related to the accumulation of rainwater

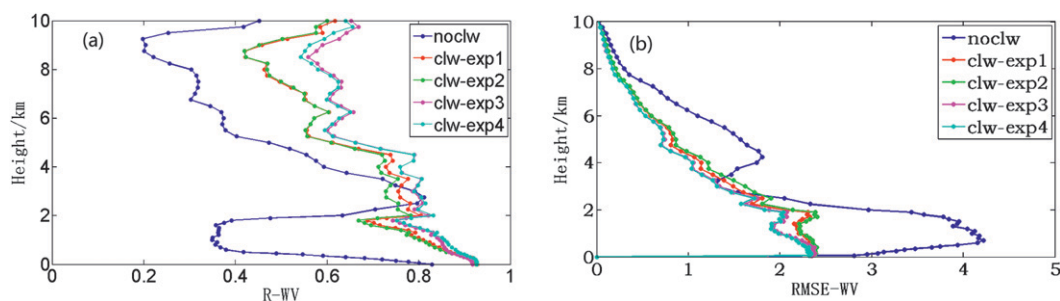


FIG. 8. The impact of different prescribed forms of cloud liquid water profile on the retrieval of vertical profile of water vapor density.

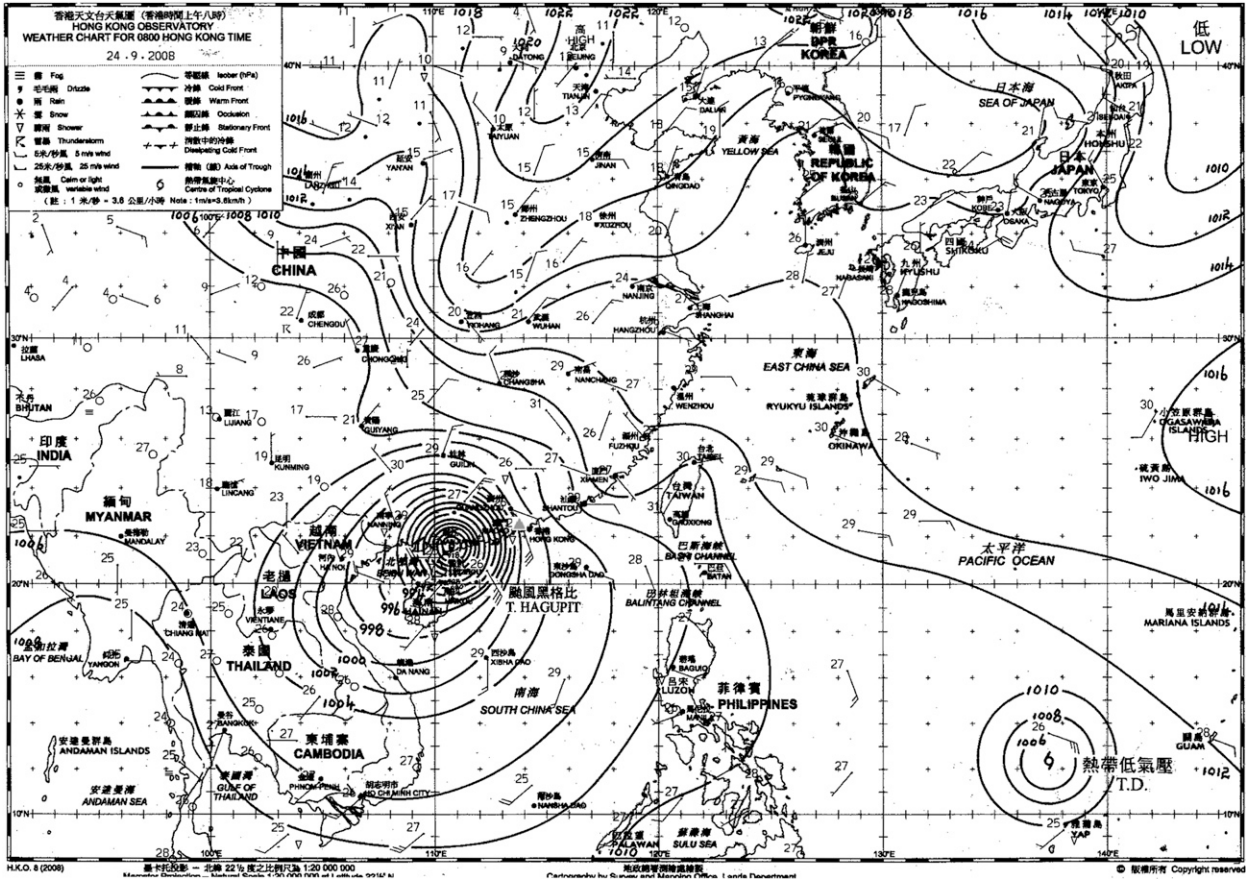


FIG. 9. Surface isobaric chart at 0000 UTC 24 Sep 2008.

on the radome of the radiometer, which caused significant deviations of the measured K-band brightness temperatures from the actual values. Though the radome is made with hydrophobic materials and there is a blower to keep the rainwater away, there could still be a residual amount of rainwater on the radome in heavy rain situations. It could be seen from Fig. 10h that there were rapid fluctuations of the measured K-band brightness temperatures in the above-mentioned period. Such fluctuations did not appear to be simply due to changes in the atmospheric conditions. Rainwater accumulation on the radome surface could play a significant role here.

The performance of the RNN algorithm is also considered. The time–height plot of the water vapor density is given in Fig. 10d. Compared to Fig. 10c (the results of the PSR method), it appears that the results from the RNN method do not seem to be quite reasonable; at the least there are significant variations of the retrieved water vapor density with height. The vertical profiles of water vapor density from the two methods are compared with the radiosonde profile in Fig. 10e. It could be seen

that the result from the PSR method is much more reasonable in comparison with the radiosonde data.

A monsoon surge of cold air reached southern China in the period of 7–9 November 2008. The surface isobaric chart is shown in Fig. 11. Figure 12 shows that the temperature decreased from 7 to 9 November. There was diurnal temperature variation on each day. The water vapor density and relative humidity were relatively low in this season. After the arrival of the cold surge, the water vapor density and relative humidity over the troposphere decreased further. During the passage of the cold front, namely, 1400–1500 UTC 7 November 2008, the warmer and more humid air originally affecting southern China was made to lift, resulting in saturation of the lower troposphere and thus occurrence of frontal rain.

6. Discussions and conclusions

This paper uses the radiosonde data in Hong Kong in the period from June 2003 to September 2009 and MonoRTM to establish the retrieval algorithm for a 35-channel, ground-based microwave radiometer. The

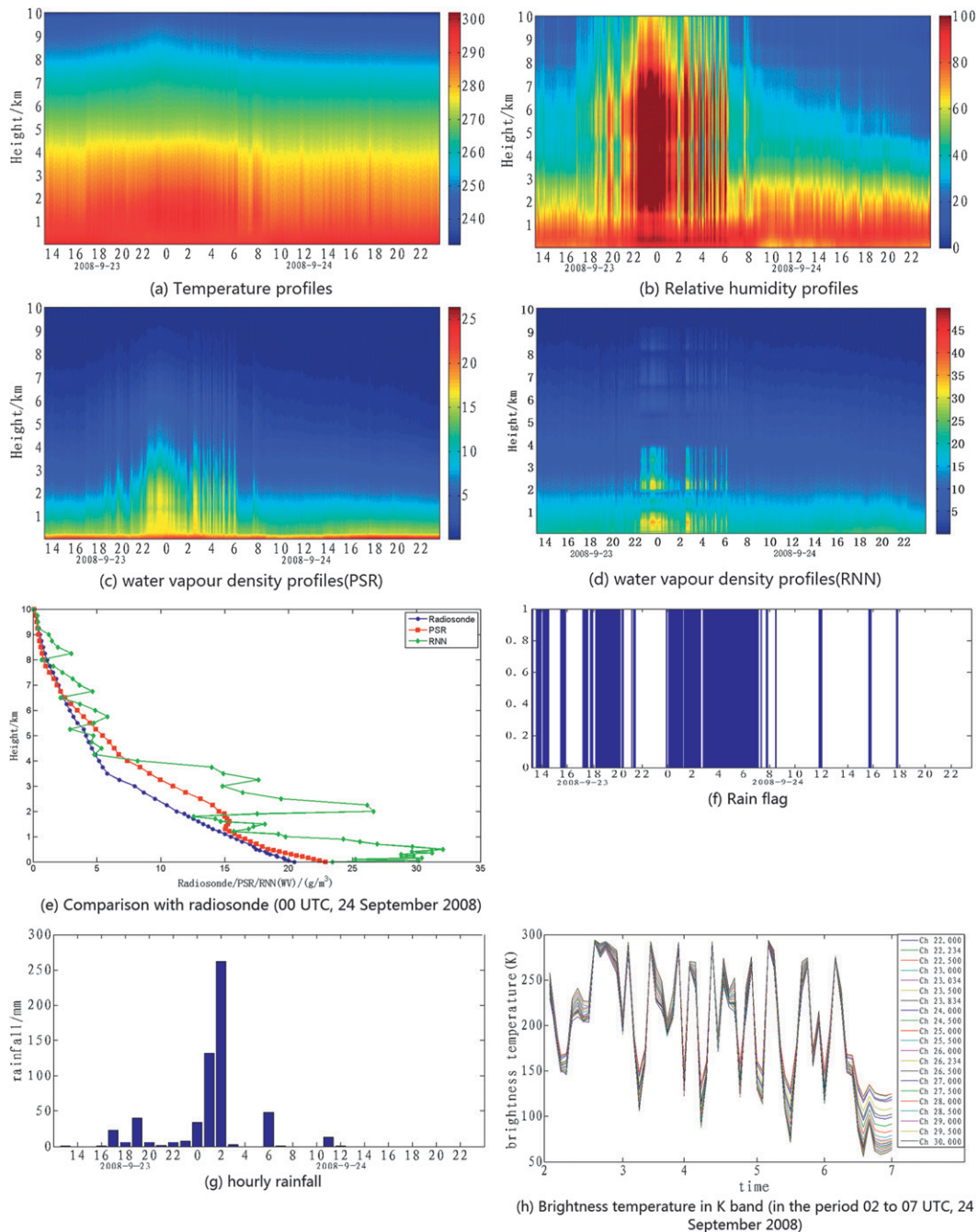


FIG. 10. Meteorological data at Nansha in the period 23–24 Sep 2008: (a) temperature profiles, (b) relative humidity profiles, (c) water vapor density profiles (PSR), (d) water vapor density profiles (RNN), (e) comparison with radiosonde (0000 UTC 24 Sep 2008), (f) rain detector data, (g) hourly rainfall, and (h) K-band brightness temperature.

relationship between the measured brightness temperatures and the retrieved temperature–humidity profiles is built up based on principal component analysis and stepwise regression.

As verified with an independent data sample, the retrieved temperatures have an RMSE generally less than

1.5 K with the retrieval results performing better in summer than in winter. The retrieved water vapor density has a larger RMSE of 1.4 g m^{-3} at heights of 0.5–2 km and achieves an error below 1 g m^{-3} at the other heights. Considering that Hong Kong has relatively large amount of water vapor over the year, the above errors with the

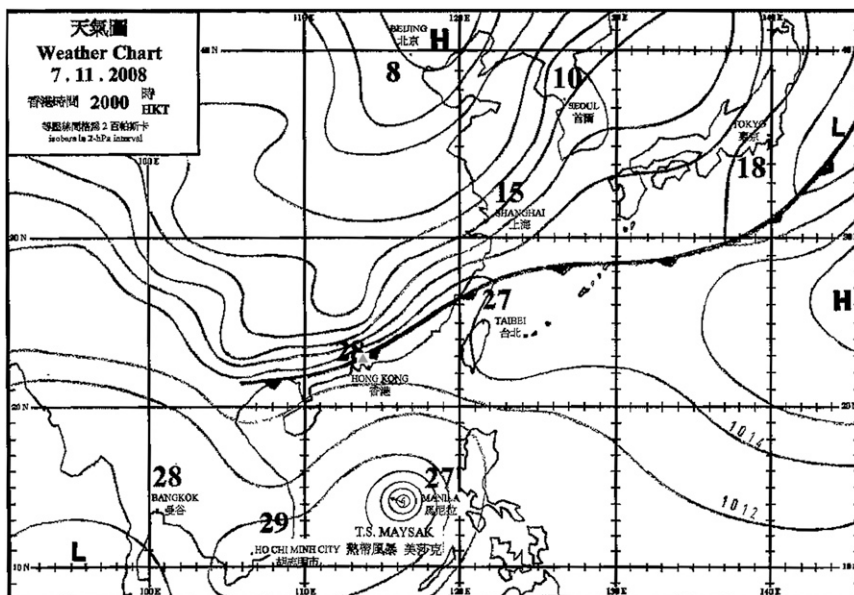


FIG. 11. Surface isobaric chart at 1200 UTC 7 Nov 2008.

retrieved water vapor density is regarded as acceptable. Using the actual radiometer measurements at Nansha for retrieval and comparison with the results of the RNN method, as supplied with the radiometer, it is found that the PSR method is generally more accurate than the RNN method for the retrieval of temperature and relative humidity profiles, whereas the errors are comparable for the two methods in the retrieval of water vapor density. By using numerical experiments, the prescribed

cloud liquid water profile is found to have a significant impact on the quality of the retrieved water vapor density profile, and the uncertainty with the former profile is a major source of error in recovering the water vapor density profile. Finally, using actual radiometer measurements, the retrieved method as discussed in this paper is shown to capture successfully the evolution of the thermodynamic profiles of the troposphere in two typical weather events over southern China, namely, the

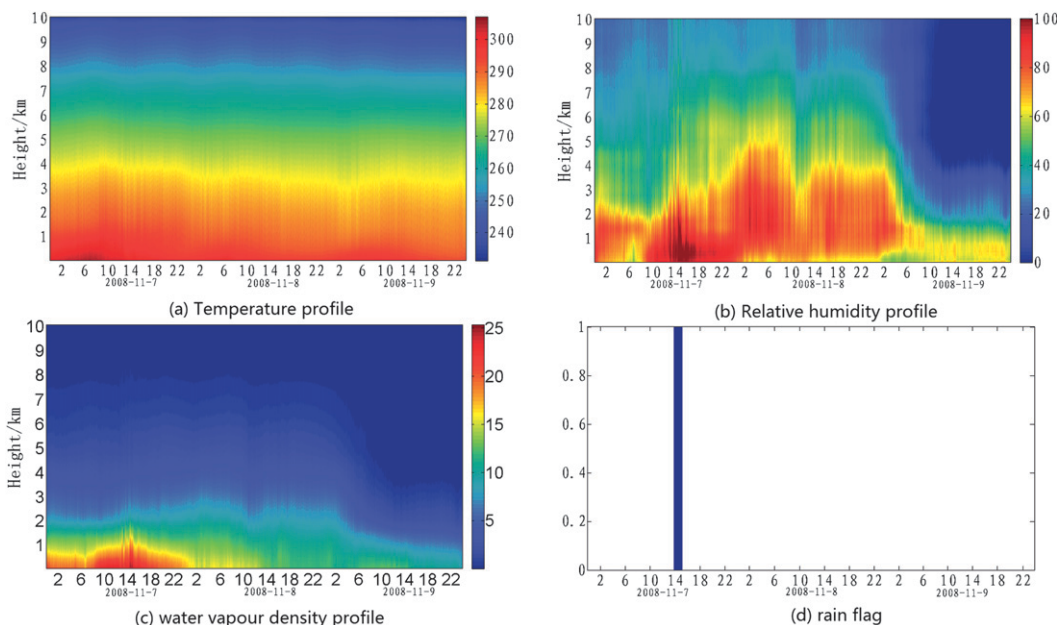


FIG. 12. Weather data at Nansha in the period of 7–9 Nov 2008: (a) temperature profiles, (b) relative humidity profiles, (c) water vapor density profiles, and (d) rain detector data.

passage of a typhoon (Hagupit) and the arrival of cold monsoon surge from the north.

The quality of retrieved thermodynamic profiles of the troposphere for a ground-based microwave radiometer depends on a number of factors, namely, the amount of historical data being used, the uncertainty of the brightness temperature measurement, the radiative transfer model, the statistical model, etc. The following studies may be undertaken in the future: 1) consideration of the historical data with higher spatial and temporal resolutions; 2) combination of data from a variety of sources (e.g., satellite and radar), and using mesoscale analysis results, for example, the input of analyzed cloud liquid water profile into the radiative transfer model, in order to improve the quality of the retrieved water vapor density profile; 3) better maintenance of the radiometer with more frequent calibrations and cleaning; and 4) inclusion of nonlinear terms in the establishment of statistical model.

Acknowledgments. The authors thank Dr. Qilin Wan for providing the microwave radiometer and radiosonde data. This research was supported by NSFC Grants 40905018 and Guangdong Natural Science Foundation under Grant 9151008019000008.

REFERENCES

- Askne, J., and E. R. Westwater, 1996: A review of ground-based remote sensing of temperature and moisture by passive microwave radiometers. *IEEE Trans. Geosci. Remote Sens.*, **24**, 340–352.
- Boukabara, S. A., S. A. Clough, and R. N. Hoffman, 1999: MonoRTM: A monochromatic radiation transfer model for microwave and laser calculations. Preprints, *22nd Annual Review Conf. on Atmospheric Transmission Models*, Hanscom Air Force Base, MA, ASFC.
- Churnside, J. H., T. A. Stermitz, and J. A. Schroeder, 1994: Temperature profiling with neural network inversion of microwave radiometer data. *J. Atmos. Oceanic Technol.*, **11**, 105–109.
- Cimini, C., F. S. Marzano, and P. Ciottiet, 2004: Atmospheric microwave radiative models study based on ground-based multichannel radiometer observations in the 20-60-ghz band. Preprints, *14th ARM Science Team Meeting Proc.*, Albuquerque, NM, ARM. [Available online at http://newdesign.arm.gov/publications/proceedings/conf14/extended_abs/cimini-d.pdf.]
- Clough, S. A., M. W. Shephard, E. J. Mlawer, J. S. Delamere, M. J. Iacono, K. Cady-Pereira, S. Boukabara, and P. D. Brown, 2005: Atmospheric radiative transfer modeling: A summary of the AER codes. *J. Quant. Spectrosc. Radiat. Transfer*, **91**, 233–244.
- Duan, Y., and Z. Wu, 1999: Monitoring the distribution characteristics of liquid and vapour water content in the atmosphere using ground based remote sensing (in Chinese). *J. Appl. Meteor. Sci.*, **10**, 34–40.
- Guldner, J., and D. Spankuch, 2001: Remote sensing of the thermodynamic state of the atmospheric boundary layer by ground-based microwave radiometry. *J. Atmos. Oceanic Technol.*, **18**, 925–933.
- Hewison, T., 2007: 1D-VAR retrieval of temperature and humidity profiles from ground-based microwave radiometers. *IEEE Trans. Geosci. Remote Sens.*, **45**, 2163–2168.
- Hogg, D. C., and Coauthors, 1983a: An automatic profiler of the temperature, wind, and humidity in the troposphere. *J. Climate Appl. Meteor.*, **22**, 126–133.
- , F. O. Guiraud, J. B. Snider, M. T. Decker, and E. R. Westwater, 1983b: A steerable dual-channel microwave radiometer for measurement of water vapor and liquid in the troposphere. *J. Climate Appl. Meteor.*, **22**, 789–806.
- Ledskam, W. M., and D. H. Staelin, 1978: An extended Kalman-Bucy filter for atmospheric temperature profile retrieval with a passive microwave sounder. *J. Appl. Meteor.*, **17**, 1023–1033.
- Liljegren, J. C., 2000: Automatic self-calibration of ARM microwave radiometers. *Microwave Radiometry and Remote Sensing of the Earth's Surface and Atmosphere*, P. Pampaloni and S. Paloscia, Eds., VSP Press, 433–441.
- , S.-A. Boukabara, K. Cady-Pereira, and S. A. Clough, 2004: The effect of the half-width of the 22-GHz water vapor line on retrievals of temperature and water vapor profiles with a twelve-channel microwave radiometer. *IEEE Trans. Geosci. Remote Sens.*, **43**, 1102–1108.
- Lin, L., J. Zhang, and Y. Shi, 1997: Utilizing genetic algorithms inverting atmospheric vertical temperature structure (in Chinese). *J. Grad. Sch. Chin. Acad. Sci.*, **14**, 43–50.
- Liu, H., J. Li, X. Cao, and B. Xiong, 2007: Characteristics of the atmosphere remote sensed by the ground-based 12-channel radiometer (in Chinese). *Remote Sens. Technol. Appl.*, **22**, 222–229.
- Lu, D., C. Wei, and M. Xi, 1993: A universal regressive relationship for ground-based microwave remote sensing of atmospheric precipitable water vapor (in Chinese). *Chin. J. Atmos. Sci.*, **17**, 721–731.
- Marzano, F. S., E. Fionda, P. Ciotti, and A. Martellucci, 2002: Ground-based multifrequency microwave radiometry for rainfall remote sensing. *IEEE Trans. Geosci. Remote Sens.*, **40**, 742–759.
- Phillips, N. A., L. M. McMillin, D. Wark, and A. Gruber, 1979: An evaluation of early operational temperature soundings from TIROS-N. *Bull. Amer. Meteor. Soc.*, **60**, 1188–1197.
- Shi, N., 2002: *Multiplex Analytic Method in Atmospheric Scientific Research and Prediction* (in Chinese). Atmospheric Publishing Company, 244 pp.
- Solheim, F., J. R. Godwin, E. R. Westwater, Y. Han, S. J. Keihm, K. Marsh, and R. Ware, 1998: Radiometric profiling of temperature, water vapor and cloud liquid water using various inversion methods. *Radio Sci.*, **33**, 393–404.
- Wang, Z., P. Xu, J. Deng, and W. Yan, 1995: Simulation of atmospheric vapor, liquid water content, and excess propagation path length based on a 3-channel microwave radiometer sensings (in Chinese). *J. Nanjing Inst. Meteor.*, **18**, 396–403.
- Ware, R., R. Carpenter, J. Guldner, J. Liljegren, T. Nehr Korn, F. Solheim, and F. Vandenberghe, 2003: A Multi-Channel Radiometric Profiler of Temperature, Humidity and Cloud Liquid. *Radio Sci.*, **38**, 8079, doi:10.1029/2002RS002856.
- Wei, C., and D. Lu, 1994: A universal regression retrieval method of the ground-based microwave remote sensing of precipitable water vapor and path, integrated cloud liquid water content (in Chinese). *Atmos. Res.*, **34**, 309–322.
- Westwater, E. R., S. Crewell, and C. Matzler, 2004: Frontiers in surface-based microwave and millimeter wavelength radiometry. *Proc. 2004 IEEE Int. Geoscience and Remote Sensing Symp.*, Vol. 2, Anchorage, AK, IEEE, 1268–1272.

- , —, and —, 2005a: Surface-based microwave and millimeter wave radiometric remote sensing of the troposphere: A tutorial. *J. IEEE Geoscience and Remote Sensing Society Newsletter*, No. 134, IEEE, 16–33.
- , —, —, and D. Cimini, 2005b: Principles of surface-based microwave and millimeter wave radiometric remote sensing of the troposphere. *Quad. Soc. Ital. Elettromagnetismo*, **1**, 50–90.
- Wu, D., 1987a: The cloud droplet spectral feature of precipitous stratified clouds from June to July in Ningxia (in Chinese). *J. Meteor. Mon.*, **13**, 48–50.
- , 1987b: The macroscopic feature of precipitous stratified clouds from May to August in Ningxia (in Chinese). *J. Plateau Meteor.*, **6**, 170–175.
- , Y. He, G. Chen, R. Chen, S. He, X. Wei, and G. He, 1998: The microphysical features of warm clouds over the Xinfeng Jiang River Valley in Guangdong (in Chinese). *J. Trop. Meteor.*, **4**, 341–349.
- Zhao, B., and Coauthors, 1984: A experimental study on multi-channel microwave remote sensing of atmospheric structure (in Chinese). *Sci. China*, **11B**, 1059–1066.